JCTC Journal of Chemical Theory and Computation

The Importance of Going beyond Coulombic Potential in Embedding Calculations for Molecular Properties: The Case of Iso-G for Biliverdin in Protein-Like Environment

Georgios Fradelos and Tomasz A. Wesolowski*

Université de Genève, Département de Chimie Physique 30, quai Ernest-Ansermet, CH-1211 Genève 4, Switzerland

Received July 23, 2010

Abstract: The importance of the nonelectrostatic component of the embedding potential is investigated by comparing the complexation induced shifts of the iso-g obtained in embedding calculations to its supermolecular counterparts. The analyses are made in view of such multilevel simulations, for which supermolecular strategy is either impractical or impossible, such as the planned simulations for the whole enzyme ferredoxin oxidoreductase. For the biliverdin radical surrounded by a few amino acids, it is shown that the embedding potential comprising only Coulomb terms fails to reproduce even qualitatively the shifts evaluated from supermolecular calculations. The nonelectrostatic component of the exact embedding potential is a bifunctional of two electron densities [Wesolowski and Warshel, *J. Phys. Chem.* **1993**, *97*, 8050; Wesolowski, *Phys. Rev. A* **2008**, *77*, 012504]. Therefore we analyze in detail both the quality of the approximant for the bifunctional and the importance of the choice of the electron densities at which it is evaluated in practical calculations.

Introduction

Multilevel techniques in numerical simulation apply the embedding potential to couple the subsystem described at the quantum mechanical level with its environment described using simpler descriptors. If the quantum mechanical treatment of the whole system under investigation is impractical or impossible, then such techniques are the only options available. Such approaches are frequently referred as quantum mechanical/molecular mechanical (QM/MM)[1] and are widely applied in simulation of biomolecules,[2,3] materials,[4] liquids,[5] solids,[6,7] and interfaces,[8] for instance. The embedding potential, i.e., the potential added to the potential in the environment-free case, $v_0(\vec{r})$, is commonly represented by the electrostatic potential (atomic units are applied in all the equations given in the present work):

$$v^{\mathrm{eff}}_{\mathrm{emb(Coulomb)}}[\rho_A, \rho_B; \vec{r}] = v^{B}_{\mathrm{ext}}(\vec{r}) + \int \frac{\rho_B(\vec{r}')}{|\vec{r}' - \vec{r}|} \mathrm{d}\vec{r}' \quad (1)$$

The convention used in eq 1 indicating that the embedding potential is a functional of the two electron densities ρ_A (the electron density of the embedded system) and ρ_B (the electron density of the environment) and is used for the sake of the subsequent discussions. Note that the embedding potential given in eq 1 does not depend on ρ_A, i.e., the electron density of the embedded system. In practice, the second term representing the classical Coulomb electron−electron repulsion is evaluated using truncated polycenter multipole expansion. Especially simple is the case of the expansion truncated to monopoles, which leads to a very efficient computational method where the nuclear and monopole expansion charges can be bunched together giving rise to a set of distributed effective charges.

The potential given in eq 1 does not take into account the nonelectrostatic effects on the electronic structure of the embedded species which arise from the Pauli exclusion principle (see ref 9 for discussion of this issue in a model system). If such effects cannot be neglected, then the straightforward solution is to add to the electrostatic potential a nonlocal component consisting of projection operators (or simplified molecular pseudopotentials),[10] which hinges on

* Corresponding author. E-mail: tomasz.wesolowski@unige.ch. Telephone: 041223796101.

10.1021/ct100415h
Published on Web 12/07/2010

the availability of the orbitals for the environment. In multilevel simulations, such as QM/MM, etc., especially if the target is not a property directly related to the electronic structure but to the potential energy surface, the nonelectrostatic component of the exact embedding potential is frequently neglected, resulting in an inexpensive computational approach. In such a case, the deficiencies of electrostatic-only embedding potentials can be corrected by special terms added to the final expression for the total energy.[11−15] Such corrections are, however, strongly system and method dependent as pointed out by several authors. For instance, the authors of a recent review state that, "QM/MM calculations are not yet black-box procedures",[16] and the authors of ref 17 conclude that "...the need to partition the complete system into regions treated at different levels of theory, and to allow these regions to interact, creates two significant problems. First is the treatment of the QM/MM boundary, as it is often necessary to place this boundary across covalent bonds. Second is the parameterization of the hybrid system Hamiltonian." Several authors reported problems, such as excess polarization of the embedded subsystem by the environment, when the embedding potential comprises only electrostatic terms.[18−20] Specific numerical problems arising from neglecting nonelectrostatic terms in the embedding potential, especially if the basis set used to construct embedded orbitals extends into the environment, were also reported.[21−23] In numerical simulations aiming at obtaining properties of embedded systems, which are other than ground-state energy, the large basis sets are frequently indispensable. Therefore, the quality of the calculated values depends directly on the accuracy of the used embedding potential. The pragmatic solution made for the ground-state energy, i.e., as adding a correction term directly to the energy, is less straightforward for other observables. To correct errors for such quantities, the cure must be applied to the embedding potential, as it determines the quality of the calculated electronic structure.

The frozen-density embedding theory (FDET)[24−28] provides a formal basis for computational methods (besides our own work see also other representative papers)[29−33] in which both the energy as well as the electronic properties are evaluated in a self-consistent manner. Below, we outline the basic elements of the frozen-density embedding theory:

- **Basic variables.** The total investigated system is characterized by two quantities: the density $\rho_B(\vec{r})$, which for a given electronic problem is a frozen function, and the density $\rho_A(\vec{r})$, which is represented using auxiliary quantities, such as occupied orbitals of noninteracting reference system $\{\phi_A^i(\vec{r})\}$,[24] occupied and unoccupied orbitals of noninteracting reference system,[25] interacting wave function,[27] or one-particle density matrix.[28]
- **Constrained search.** The density $\rho_A(\vec{r})$ is obtained by performing the following search:

$$\begin{aligned} E_{\mathrm{emb}}[\rho_B] &= \min_{\rho_A \geq 0} E^{HK}[\rho_A + \rho_B] \text{ for } \int \rho_A(\vec{r})\mathrm{d}\vec{r} = N_A \\ &= \min_{\rho \geq \rho_B \geq 0} E^{HK}[\rho] \text{ for } \int \rho_B(\vec{r})\mathrm{d}\vec{r} = N_B \end{aligned} \quad (2)$$

- **Performing the constrained search by modifying the external potential.** The search is conducted in practice by solving the following equation:

$$(\hat{H}_o + \hat{v}_{\mathrm{emb}})\psi = E_{\mathrm{emb}}\psi \quad (3)$$

where $\hat{H}_o$ is the environment-free Hamiltonian, and the $\hat{v}_{\mathrm{emb}}(\vec{r})$ has the form of a local potential ($v_{\mathrm{emb}}^{\mathrm{eff}}(\vec{r})$), which is determined by the pair of densities $\rho_A(\vec{r})$ and $\rho_B(\vec{r})$, hence orbital-free embedding.

- **Orbital-free embedding potential.** The form of the dependence of the embedding potential on the densities $\rho_A(\vec{r})$ and $\rho_B(\vec{r})$ depends on what QM descriptor is used as the auxiliary quantity for $\rho_A(\vec{r})$ and is given in respective publications.[24,27,28] For the following descriptors: orbitals of noninteracting reference system, a wave function of the full configuration interaction form, and one-particle density matrix, the orbital-free embedding potential reads:

$$\begin{aligned} v_{\mathrm{emb}}^{\mathrm{eff}}[\rho_A, \rho_B; \vec{r}] = v_{\mathrm{ext}}^{B}(\vec{r}) + \int \frac{\rho_B(\vec{r}')}{|\vec{r}' - \vec{r}|}\mathrm{d}\vec{r}' + \left.\frac{\delta E_{\mathrm{xc}}[\rho]}{\delta \rho}\right|_{\rho=\rho_A+\rho_B} - \\ \left.\frac{\delta E_{\mathrm{xc}}[\rho]}{\delta \rho}\right|_{\rho=\rho_A} + \left.\frac{\delta T_s[\rho]}{\delta \rho}\right|_{\rho=\rho_A+\rho_B} - \left.\frac{\delta T_s[\rho]}{\delta \rho}\right|_{\rho=\rho_A} \end{aligned} \quad (4)$$

The correspondence given in eq 4 involves density functionals known in the Kohn−Sham formulation[34] of density functional theory,[35] the functional of the exchange−correlation energy ($E_{\mathrm{xc}}[\rho]$), and the functional of the kinetic energy in a noninteracting system ($T_s[\rho]$). The pair of functional derivatives of the functional $T_s[\rho]$ arises from from nonadditivity of this functional and represents a potential denoted as $v_t^{\mathrm{nad}}[\rho_A, \rho_B](\vec{r})$ in the present work.

In this context, it is useful to relate the frozen-density embedding theory to the subsystem formulation of density functional theory (SDFT)[36,37] and to the recently developed partition density functional theory (PDFT).[38] Both SDFT and PDFT lead to the exact ground-state electron density and the energy of the whole investigated system an alternative way to the conventional Kohn−Sham framework. In SDFT, the charges of each subsystem are assumed to be integral (similarly as in FDET), whereas fractional charges of subsystems are allowed in PDFT. The FDET targets not the ground-state electron density of the total system but the density minimizing the Hohenberg−Kohn energy functional for the total system with the presence of constraints. FDET, therefore, can lead to the same total ground-state density as SDFT and Kohn−Sham DFT or PDFT, only when for particular constraints[26] (see also below). In the case of two subsystems, SDFT is based on the following variational principle:

$$E_o = \min_{\rho_A \geq 0, \rho_B \geq 0} E^{HK}[\rho_A + \rho_B] \text{ for } \int \rho_A(\vec{r})\mathrm{d}\vec{r} = N_A, \int \rho_B(\vec{r})\mathrm{d}\vec{r} = N_B \quad (5)$$

where the search is performed among subsystem densities which are pure-state noninteracting v-representable. The sufficient condition for reaching the exact ground-state

density in SDFT is that it can be decomposed as a sum of two pure-state noninteracting v-representable densities comprising an integer number of electrons N_A and N_B (see the discussions in ref 26). FDET does not target the ground-state of the total system but the density, which minimizes the total ground-state energy in presence of the following constraint:

$$\rho \geq \rho_B \tag{6}$$

which is given in advance.

The total density obtained in FDET (eq 2 is, therefore, not equal to the exact ground-state density except for a particular case, i.e., when the difference between $\rho_o^{tot}(\vec{r})$ and the assumed $\rho_B(\vec{r})$ is representable using one of the auxiliary descriptors mentioned above: orbitals of the noninteracting reference system,[24] interacting wave function,[27] or one particle density matrix.[28] On the virtue of Hohenberg−Kohn theorems, FDET can lead only to the upper bound of the ground-state energy:

$$E_{emb}[\rho_B] \geq E_o \tag{7}$$

Any numerical implementation of FDET can be easily converted to methods solving coupled Kohn−Sham-like equations in SDFT. In fact, the first numerical implementation of SDFT applicable for molecular systems used the "freeze-and-thaw" cycle,[39] which was applied in a number of subsequent studies (see for instance refs 40−42). In the original numerical studies based on SDFT concerning atoms in solids[36,37] and in the recent numerical implementation of SDFT for molecular liquids,[43] the coupled Kohn−Sham equations are solved simultaneously. We have also shown recently that the "freeze-and-thaw" cycle can be performed simultaneously with displacing nuclear position accelerating the SDFT-based geometry optimization.[44] The "freeze-and-thaw" cycle to solve the coupled Kohn−Sham like equations is used by us in methodological studies on approximants to the bifunctional of the nonadditive kinetic potential $v_t^{nad}[\rho_A, \rho_B]$ (see for instance refs 45−47) or in preparation stages for large-scale simulations, in which the search given in eq 2 is performed for smaller model systems in order to establish the adequacy of the simplified $\rho_B(\vec{r})$ in large-scale simulations.

If a noninteracting reference system is used to perform the search given in eq 2, the corresponding orbitals (ϕ_i^A) are obtained from the following Kohn−Sham-like equations (eqs 20−21 in ref 24):

$$\left[-\frac{1}{2}\nabla^2 + v_{eff}^{KS}[\rho_A, \vec{r}] + v_{emb}^{eff}[\rho_A, \rho_B; \vec{r}]\right]\varphi_i^A = \varepsilon_i^A \varphi_i^A \qquad i = 1, N^A \tag{8}$$

where $v_{emb}^{eff}[\rho_A, \rho_B; \vec{r}]$ is given in eq 4.

The effectiveness of methods based on eq 8 for the studying changes in the electronic structure arising due to the interactions between the embedded system and its environment was demonstrated for: vertical excitation energies,[25,48] electron spin resonance (ESR) hyperfine coupling constants,[49,50] ligand-field splittings of f-levels in lanthanide impurities,[51] NMR shieldings,[52] dipole and quadrupole moments, electronic excitation energies, and frequency dependent polarizabilities.[53]

In multilevel simulations based on FDET, ρ_B is an assumed quantity, which can obtained following various approaches. Since the electron density is a well-defined quantity also in the macroscale, it is even possible to generate ρ_B without using any quantum chemical approach.[54] A natural choice for ρ_B is to use Kohn−Sham equations to generate it for the isolated environment and to use it for generating the embedding potential. Such procedure does not take into account the electronic polarization of the environment by the embedded subsystem. For this reason such density and embedding potential are labeled as nonrelaxed. If the "freeze-and-thaw" procedure[55] is used to generate ρ_B, which together with the optimal ρ_A minimizes the energy of the whole system, then the corresponding quantities are labeled as relaxed.

Our own numerical experience concerning the applicability of eq 1 in embedding calculations shows invariably that it leads frequently to qualitatively wrong or erratic results, especially if other properties than energy are investigated (for ligand field splitting of the f-levels for lanthanide impurities in solids see ref 51, for redistribution of electron density in charged intermolecular complexes see ref 56, for electron density and total energy in intermolecular complexes see ref 45, for excitation energies see ref 25, for instance). The erratic results obtained using the electrostatic-only embedding potential arise from the fact that any variational method neglecting nonelectrostatic terms neither assures the proper variational limit in the sense of the second Hohenberg−Kohn theorem nor takes into account the antisymmetric character of the wave function for the whole system. The present work represents an extension of such studies. A systematic account of the flaws of the electrostatic-only embedding potential is provided for yet another quantity directly related to the electronic structure—the values of iso-g for an embedded radical molecule. The g-tensor is an important parameter of ESR spectroscopy, and its analysis is used as a supplementary tool to elucidate the protonation state of a radical in the enzyme's active center.[57] The protein provides both the steric constraints affecting the geometry of the radical as well as the electronic environment (long-range electrostatic as well as short-range Pauli repulsion), which affect the observed g-tensor. Modeling g-tensor must take a proper account of these two types of effects, and the FDET methods are especially designed to study the electronic effects (for a representative study see ref 50). The secondary aim of this study is the analysis of the errors in calculated environment-induced shifts of iso-g which can be attributed to the use of approximate density functional for the nonadditive kinetic potential $v_t^{nad}[\rho_A, \rho_B]$, i.e., the last two terms in eq 4.

We have chosen to study a model system consisting of the biliverdin IXa radical (BV) and a few amino acids of the protein phycocyanobilin (PCYA) representing the nearest neighbors of BV in the BV−PCYA complex. The g-tensor of BV has extremely small anisotropy. It should be noted that conventional ESR cannot resolve the components of g-tensors with very small anisotropy (as those of organic

radicals), but recent developments in high-field ESR allow one to determine the components of even such g-tensors and to use them in the interpretation of biochemical data.[57] It is known that PCYA catalyzes the reduction of BV to PCYA, the precursor of biliprotein chromophores found in phycobilisomes. The present work represents the preparatory stage of the project aimed at studying the whole protein−radical complex by means of multilevel type of simulations based on FDET. Two numerical model related issues: the adequacy of the used the approximant for the bifunctional of the nonelectrostatic components of the embedding potential and the adequacy of the choice for ρ_B are, therefore, at the focus of the present work.

In order to obtain the absolute values of iso-g as and the environment induced shifts of this quantity [Δiso-g = iso-g(BV + environment) − iso-g(BV)], the calculations based on either embedding or supermolecular strategy are feasible for the investigated model system, which is rather small. The possible advantages of using the FDET-based embedding calculations over the supermolecular ones lie not only in reducing the computational costs. If the shifts arise from nonbonding interactions between the embedded molecule and its environment, then the quality of the shifts obtained from FDET strategy can be expected to be better than their supermolecular counterparts for the reasons addressed in more detail below. The quality of the results obtained in both the Kohn−Sham and the embedding calculations depend on such common factors as: (a) the molecular model of the real system (size of the model and coordinates of atoms not available from experiments), (b) the approximant for the exchange−correlation functional, (c) the treatment of relativistic effects (the spin−orbit coupling in particular), and (d) the basis set. As far as the environment induced shifts are concerned, however, their quality in supermolecular and embedding calculations is determined by different factors. In the supermolecular case, the shift is the difference between values obtained from two independent Kohn−Sham calculations. As a result, the errors in iso-g might cumulate or cancel. In the embedding case, the calculated shift arises from the addition of the embedding potential to the effective potential corresponding to the system without any environment. The errors in the shifts are, therefore, determined mainly by the quality of the embedding potential given in eq 4. Due to its first-principles based origin, the quality of the embedding potential used in practice is determined by only two factors: the chosen frozen electron density (ρ_B) and the used approximant for the nonadditive kinetic potential (the last two terms in eq 4). The importance of the first factor can be easily monitored by performing the "freeze-and-thaw" calculations on model systems. Concerning the orbital-free embedding potential expressed as the functional of ρ_A and ρ_B, its medium- and long-range part is known exactly (electrostatics) and can be expected to dominate if the embedded molecule is surrounded by noncovalently bound polar molecules. Since the errors in the shifts of the properties related directly to the electronic structure, i.e., to the embedded orbitals and their energies, are determined only by the accuracy of the approximants to the nonadditive kinetic− and exchange−correlation potentials, one can expect that, whenever the environment includes polar or charged molecules represented exactly in the orbital-free embedding potential given in eq 4, the shifts obtained from FDET-based calculations surpass in accuracy the ones derived using their supermolecular counterparts.

The model environment of BV considered in the present work is the same as the one investigated earlier in the study aimed at determination of the protonation state of PCYA−bound BV,[57] where the supermolecular calculations were used to interpret experimental data. We use the same model for different purposes: (a) to explore the possibility of replacing supermolecular calculations by embedding ones for these types of analyses and (b) to determine the necessary conditions (choice of the frozen density, number of centers to expand the embedded orbitals using atomic bases, possibility to neglect nonelectrostatic components of the exact orbital-free embedding potential) for the optimal embedding calculations, i.e., assuring the smallest of the deviations from the supermolecular results at the largest reduction of the computational efforts.

Computational Details

The three considered protonation states denoted with $\alpha ACD\delta^{\bullet+}$, $ACD\delta^{\bullet}$, $ACD^{\bullet-}$ are shown in Figure 1. In the label, a big letter indicates a protonated nitrogen site in the pyrrole ring (A, B, C, or D), a Greek letter (α or δ) denotes a protonated carbonyl oxygen site, and the + or − denote the charge of the embedded species.

Two cluster models of the environment of the PCYA−bound BV shown in Figure 2 are considered: the smaller (EHD) and the larger (EHDYQ) (the amino acids are referred to with commonly used one letter codes). The EHDYQ cluster comprises amino acids: GLU76, HIS88, ASP105, TYR212, and GLN216 in their neutral form taken from the 2D1E structure deposited in the Protein Data Bank (PDB).[58] The EHD cluster comprises GLU76, HIS88, and ASP105 (all polar). These three amino acids are chosen because of their proximity to the carbonyl oxygen atoms on the pyrolle rings. All of them are capable of hydrogen bonding to the protonated BV and are thus critical for determining the locations of protons in BV. They are expected to affect the g-tensor of the protein-bound BV. The amino acids of the EHD cluster are also believed to be essential in catalysis as proton donors.[59] Concerning the larger cluster (EHDYQ), it comprises additionally to two polar amino acids TYR212 and GLN216. They are near the α carbonyl oxygen atom of the pyrrole ring and far from the δ carbonyl oxygen atom.

The position of the hydrogen atoms, which is not available in the PDB structure, was generated initially using "Accelrys DS Visualizer suite"[60] and subsequently refined using the nonrelativistic Kohn−Sham LDA calculations, with the STO-type triple-ζ with polarization functions basis sets (TZP label in the ADF version 2009.01 basis set library). The Cartesian coordinates are provided in the Supporting Information.

The g-tensor, the main property investigated in the present work, is related to the magnetic moment of an electron as: $\mu = -g\beta S$ where S is the electron spin, and β the bohr magneton. The g-value depends on the particular magnetic species under consideration.[65] The principal components of

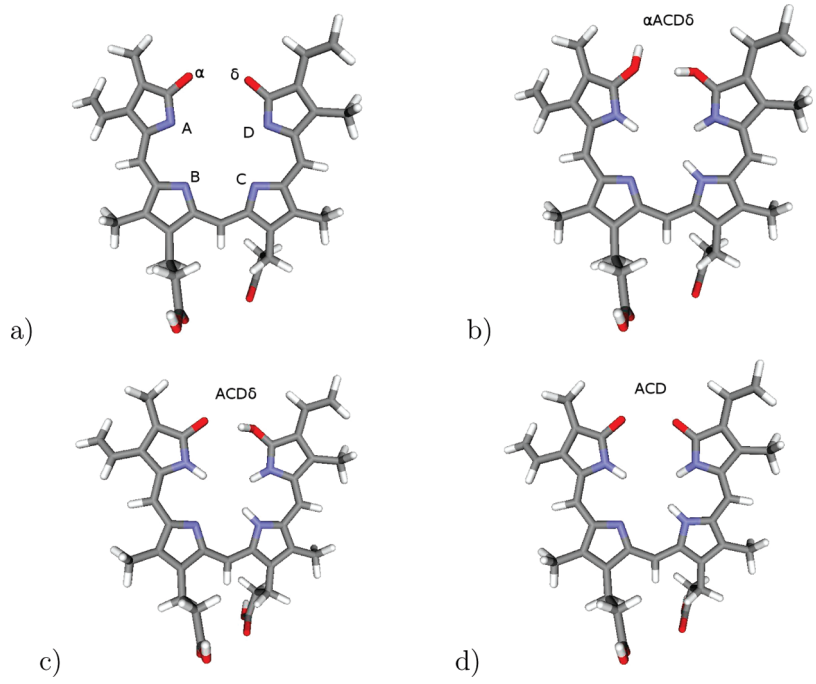

Figure 1. (a) The six positions in the BV IXa radical that can be protonated: α, δ, A, B, C, and D. The three considered protonation states: (b) αACD$\delta^{\bullet+}$, (c) ACD$\delta^{\bullet}$, and d) ACD$^{\bullet-}$.

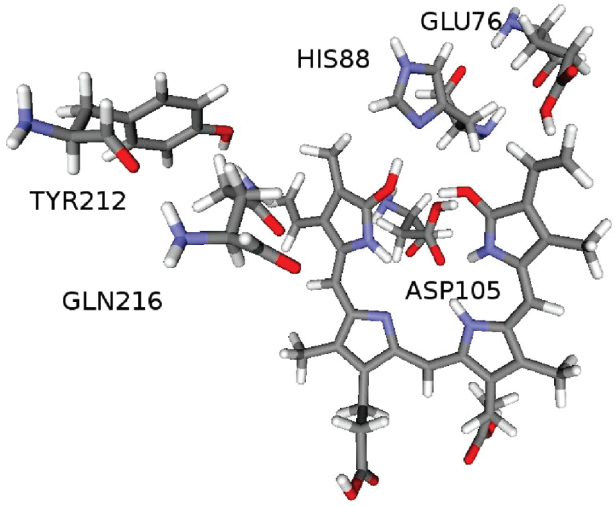

Figure 2. BV IXa in the αACD$\delta^{\bullet+}$ protonation state (for the convention, see Figure 1) in ferredoxin oxidoreductase represented by five amino acids: GLU76, HIS88, ASP105, TYR212, and GLN216.

the g-tensor together with the hyperfine tensor A specify the positions and the splittings of the lines in ESR spectra, depending on the direction of the magnetic field relative to the molecular axis. The spectral anisotropy is completely specified by three g-values (g_{xx}, g_{yy}, g_{zz}) and three hyperfine constants (A_{xx}, A_{yy}, A_{zz}). The isotropic g-value (iso-g), which is discussed throughout the present work, is the average of the principal g-values: iso-g $= 1/3(g_{xx} + g_{yy} + g_{zz})$.

In this study, the molecular g-values are calculated based on the solutions of the relativistic Kohn−Sham equations in the "spin−orbit coupling containing zeroth order regular approximation (ZORA) to the Dirac equation".[66−69] In ZORA, the spin−orbit coupling interaction (which is for many systems the most important factor for shifting the g-tensor components away from the free-electron value g_e) and other relativistic effects are taken into account variationally. The spin-restricted version of the spin−orbit including ZORA calculations,[70] which is computationally less expensive than the spin-unrestricted version[71] and thus more attractive for the study of average and big sized systems, was used. The method introduced in ref 70 combining ZORA with a single-orbital reference technique to deal with gauge dependency for open-shell doublet systems was applied.

The Becke−Perdew exchange−correlation functional[72,73] is used in both supermolecular and embedding calculations. This choice is motivated by its reported reliability in the calculation of the ESR parameters.[70]

The recently developed approximant to the nonadditive kinetic energy bifunctional (NDSD),[46] which satisfies the uniform electron gas limit and the asymptotic form of the exact bifunctional for the nonadditive kinetic potential at $\rho_A \to 0$ and $\int \rho_B d\vec{r} = 2$, was used. It takes the following form:

$$\tilde{T}_s^{\mathrm{nad(NDSD)}}[\rho_A, \rho_B] = \frac{3}{10}(3\pi^2)^{2/3} \int ((\rho_A + \rho_B)^{5/3} - \rho_A^{5/3} - \rho_B^{5/3}) d\vec{r} + \int f(\rho_B, \nabla\rho_B) \cdot \rho_A(\vec{r}) \cdot v_t^{\mathrm{limit}}[\rho_B](\vec{r}) d\vec{r} \quad (9)$$

where

$$v_t^{\mathrm{limit}}[\rho_B](\vec{r}) = \frac{1}{8}\frac{|\nabla\rho_B|^2}{\rho_B^2} - \frac{1}{4}\frac{\nabla^2\rho_B}{\rho_B} \quad (10)$$

$$f(\rho_B, \nabla\rho_B) = (\exp(\lambda(-s_B + s_B^{\min})) + 1)^{-1} \times (1 - (\exp(\lambda(-s_B + s_B^{\max})) + 1)^{-1}) \times (\exp(\lambda(-\rho_B + \rho_B^{\min})) + 1)^{-1} \quad (11)$$

and where: $s_B = (|\nabla\rho_B|)/(2(3\pi^2)^{1/3}\rho_B^{4/3})$, $s_B^{\min} = 0.3$, $s_B^{\max} = 0.9$, $\rho_B^{\min} = 0.7$, and $\lambda = 500$.

The STO-type DZP(ZORA) basis set from the ADF version 2009.01 package's basis set library,[74] that comprises a valence double-ζ basis set with one set of polarization functions, is used in the evaluation of g-tensor in both embedding and supermolecular calculations. All reported calculations are performed using the ADF version 2009.01 package.[74] Considering the atomic basis sets, it is important to point out a different significance of the choice of the number of centers used to construct molecular orbitals in supermolecular and in embedding calculations. In the supermolecular calculations, the number of centers is rarely considered an issue as they coincide with the positions of nuclei, except for some particular types of calculations. For instance, the "ghosts" are used commonly to evaluate the basis set superposition error by means of the counterpoise procedure.[61] In embedding calculations, it is natural to restrict the of centers of atomic basis sets to the nuclei of the embedded species. This is one of the sources of great computational savings in the embedding strategy after all. Addition of atomic sets localized in the environment might, however, significantly affect the numerical results of the embedding calculations.[45,46,62,63] Since eq 8 is based on variational principle (eq 2), any additional basis functions used to construct the embedded orbitals can only bring the results closer to the variational limit. The supermolecular expansion is, therefore, used as a standard in development/testing approximants for $v_t^{\mathrm{nad}}[\rho_A, \rho_B]$.[39,45,64] The use of full set of atomic centers, i.e., that in the embedded system and in the environment, is, however, not practical for large-scale simulations but is frequently applied in the preliminary stage of a simulations to chose the minimal size of the basis set and the centers assuring numerical stability for the results.[26] In the present work, the considered systems are rather small and both variants of embedding calculations are feasible. They are referred to as monomer and supermolecular expansion, respectively.

Finally, it is important to underline that to investigate the possibility of replacing the supermolecular calculations by the embedding ones using the considered embedding potentials, it is crucial that the embedding results and their supermolecular counterparts are obtained using the same: type of atomic basis sets, centers of the atomic basis sets, numerical grid, approximant for the exchange−correlation potential, and the external potential (geometry of the cluster). The particular choices for made for these quantities is of secondary importance from the point of view of the comparisons made in this work as long as the common parameters are the same in supermolecular and embedding calculations. The comparisons between the embedding and supermolecular results are made for several systems (various protonation states of BV and sizes of the environment) to ensure that the results are not accidental and to cover various possible interaction modes of a radical molecule with a protein. Nevertheless, some choices were made arbitrarily such as that for the approximant for the exchange−correlation potential, the choice of the protonation state of the amino acids, and the basis set used in most of the analysis. It is also important to underline that despite the fact that the investigated models are constructed based on the BV−PCYA complex, we do not attempt to reproduce quantitatively the experimental g-tensors because the considered models are most likely too small to be used for such purposes.

Table 1. Iso-g and Δiso-g = Iso-g(BV + Environment) − Iso-g(BV) of BV in Various Environments Calculated with Eqs 1 and 4 and Nonrelaxed Density of the Environment[a]

method[b]	environment	protonation state of BV	iso-g	Δiso-g (ppm)
embedding: eq 1[c]	EHD	αACDδ•+	2.002810	−43
embedding: eq 1[d]	EHD	αACDδ•+	NC[e]	NC[e]
embedding: eq 4[c]	EHD	αACDδ•+	2.002905	52
embedding: eq 4[d]	EHD	αACDδ•+	2.002900	47
Kohn−Sham[c]	none	αACDδ•+	2.002853	0
Kohn−Sham[d]	none	αACDδ•+	2.002849	0
Kohn−Sham	EHD	αACDδ•+	2.002928	75
embedding: eq 1[c]	EHDYQ	αACDδ•+	2.002811	−42
embedding: eq 1[d]	EHDYQ	αACDδ•+	NC[e]	NC[e]
embedding: eq 4[c]	EHDYQ	αACDδ•+	2.002904	51
embedding: eq 4[d]	EHDYQ	αACDδ•+	2.002898	45
Kohn−Sham[d]	none	αACDδ•+	2.002848	0
Kohn−Sham	EHDYQ	αACDδ•+	2.002982	129
embedding: eq 1[c]	EHD	ACDδ•	2.003639	50
embedding: eq 1[d]	EHD	ACDδ•	NC[e]	NC[e]
embedding: eq 4[c]	EHD	ACDδ•	2.003742	153
embedding: eq 4[d]	EHD	ACDδ•	2.003745	156
Kohn−Sham[c]	none	ACDδ•	2.003589	0
Kohn−Sham[d]	none	ACDδ•	2.003592	0
Kohn−Sham	EHD	ACDδ•	2.003781	192
embedding: eq 1[c]	EHD	ACD•−	2.004471	−101
embedding: eq 1[d]	EHD	ACD•−	NC[e]	NC[e]
embedding: eq 4[c]	EHD	ACD•−	2.004667	95
embedding: eq 4[d]	EHD	ACD•−	2.004661	89
Kohn−Sham[c]	none	ACD•−	2.004572	0
Kohn−Sham[d]	none	ACD•−	2.004564	0
Kohn−Sham	EHD	ACD•−	2.004494	−78

[a] Kohn−Sham results for the isolated and complexed BV are also given for reference. [b] STO-type DZP(ZORA) basis set was used. [c] Monomer basis set. [d] Supermolecular basis set. [e] Self-consistent cycle did not converge.

Results and Discussions

Throughout the results section, the environment induced shifts of the iso-g obtained from the embedding calculations are compared with the shifts obtained from the supermolecular strategy. The absolute or relative value of the difference: $\delta\Delta\text{iso-g} = \Delta\text{iso-g}^{(\text{supermolecule})} - \Delta\text{iso-g}^{(\text{embedding})}$ is used in all discussions concerning the accuracy of various embedding potentials considered in the present work. Note that the difference δΔiso-g is equal to the difference between the absolute values of iso-g calculated in supermolecular and embedding strategies ($\delta\text{iso-}g = \text{iso-g}^{\text{supermolecule}} - \text{iso-g}^{\text{embedding}}$).

Table 1 collects the iso-g and Δiso-g values obtained using nonrelaxed ρ_B for the three protonation states of BV in various environments. The reference Kohn−Sham results are also given for comparison. In three among four investigated systems, eq 1 leads to qualitatively wrong shifts (results obtained with monomer expansion). The situation is even worse when supermolecular expansion is used. The order of orbital levels is wrong, and no self-consistent solutions of eq 8 can be obtained. The situation is greatly improved if the full embedding potential given in eq 4 is used. The results of supermolecular and monomer expansion are quite similar

Table 2. Iso-g and ΔIso-g = Iso-g(BV + Environment) − Iso-g(BV) of BV in Various Environments Calculated with Eqs 1 and 4 and Relaxed Density of the Environment[a]

method[b]	environment	protonation state of BV	iso-g	Δiso-g (ppm)
embedding: eq 1[c]	EHD	αACDδ•+	2.002876	23
embedding: eq 1[d]	EHD	αACDδ•+	NC[e]	NC[e]
embedding: eq 4[c]	EHD	αACDδ•+	2.002919	66
embedding: eq 4[d]	EHD	αACDδ•+	2.002919	66
Kohn−Sham[c]	none	αACDδ•+	2.002853	0
Kohn−Sham	EHD	αACDδ•+	2.002928	75
embedding: eq 1[c]	EHDYQ	αACDδ•+	2.002883	30
embedding: eq 1[d]	EHDYQ	αACDδ•+	NC[e]	NC[e]
embedding: eq 4[c]	EHDYQ	αACDδ•+	2.002918	65
embedding: eq 4[d]	EHDYQ	αACDδ•+	2.002917	64
Kohn−Sham	EHDYQ	αACDδ•+	2.002982	129
embedding: eq 1[c]	EHD	ACDδ•	2.003629	40
embedding: eq 1[d]	EHD	ACDδ•	NC[e]	NC[e]
embedding: eq 4[c]	EHD	ACDδ•	2.003706	117
embedding: eq 4[d]	EHD	ACDδ•	2.003689	100
Kohn−Sham[c]	none	ACDδ•	2.003589	0
Kohn−Sham	EHD	ACDδ•	2.003781	192
embedding: eq 1[c]	EHD	ACD•−	2.004347	−225
embedding: eq 1[d]	EHD	ACD•−	NC[e]	NC[e]
embedding: eq 4[c]	EHD	ACD•−	2.004448	−124
embedding: eq 4[d]	EHD	ACD•−	2.004408	−164
Kohn−Sham[c]	none	ACD•−	2.004572	0
Kohn−Sham	EHD	ACD•−	2.004494	−78

[a] Kohn-Sham results for the isolated and complexed BV are also given for reference. [b] STO-type DZP(ZORA) basis set was used. [c] Monomer basis set. [d] Supermolecular basis set. [e] Self-consistent cycle did not converge.

in all cases. The complexation induced shifts obtained from embedding calculations with eq 4 reproduce qualitatively the reference values from supermolecular calculations in three considered cases but lead to qualitatively wrong shifts for $ACD^{\bullet-}$. According to the discussion in the Introduction, these discrepancies might originate from the choice of ρ_B or from the fact that an approximated functional was used for $v_t^{nad}[\rho_A, \rho_B]$. We note, however, that for embedded species which are electrically neutral, the agreement between the reference data and the shifts from the embedding calculations using the potential given in eq 4 is the best (156 vs 192 ppm). This indicates that the lack of relaxation might lie at the origin of the large discrepancies in the other cases.

To investigate this interpretation, the shifts were evaluated using the relaxed ρ_B which is obtained in the "freeze-and-thaw" procedure. They are collected in Table 2 which parallels Table 1. The relaxed ρ_B takes into account the electronic polarization of the environment by the embedded species and corresponds to the variational minimum of the total energy functional expressed using the applied approximated density functionals (SDFT). On the practical side, we notice that the "freeze-and-thaw" procedure converges rapidly and that the shifts do not change noticeably after completion of just one cycle (data not shown). Let us start with the worst case analyzed previously, i.e., $ACD^{\bullet-}$. Indeed, the qualitatively wrong complexation induced shift obtained in the absence of relaxation (+89 vs −78 ppm reference value) becomes negative (−164 ppm). The embedding potential of eq 4 leads to the correct direction of the effect but overestimates its magnitude. Removal of the basis functions localized in the environment brings the numerical result even closer to the supermolecular reference (−124 ppm). Similarly as in the nonrelaxed ρ_B case, the differences between the shifts obtained with monomer and supermolecular basis sets are significantly smaller than the magnitudes of the shifts. The situation is quite different if the electrostatic-only (eq 1) embedding potential is used. Similarly as in the previously considered nonrelaxed case, it can be noticed that the electrostatic-only embedding potential cannot be applied with supermolecular basis sets. The results obtained using the monomer expansion with the electrostatic-only embedding potential (the situation most closely resembling the typical QM/MM computational protocol) are reasonable, but they are systematically worse than the ones obtained using the full embedding potential.

Table 3. Basis Set Dependence of Iso-g and ΔIso-g = Iso-g(BV + EHD) − Iso-g(BV) Obtained in Embedding Calculations and Supermolecular (Kohn−Sham) Calculations

method[a]	basis set	iso-g	Δiso-g (ppm)
Kohn−Sham[c]	STO(DZ)	2.002959	72
Kohn−Sham[c]	STO(DZP)	2.002928	75
embedding: eq 1[b,c]	STO(DZ)	2.002871	−16
embedding: eq 1[b,c]	STO(DZ+ghosts)	NC[d]	NC[d]
embedding: eq 1[b,c]	STO(DZP)	2.002810	−43
embedding: eq 1[b,c]	STO(DZP+ghosts)	NC[d]	NC[d]
embedding: eq 1[b,d]	STO(DZ)	2.002922	35
embedding: eq 1[b,d]	STO(DZ+ghosts)	NC[d]	NC[d]
embedding: eq 1[b,d]	STO(DZP)	2.002876	23
embedding: eq 1[b,d]	STO(DZP+ghosts)	NC[d]	NC[d]
embedding: eq 4[b,c]	STO(DZ)	2.002946	59
embedding: eq 4[b,c]	STO(DZ+ghosts)	2.002938	51
embedding: eq 4[b,c]	STO(DZP)	2.002905	52
embedding: eq 4[b,c]	STO(DZP+ghosts)	2.002900	47
embedding: eq 4[b,d]	STO(DZ)	2.002959	72
embedding: eq 4[b,d]	STO(DZ+ghosts)	2.002954	67
embedding: eq 4[b,d]	STO(DZP)	2.002919	66
embedding: eq 4[b,d]	STO(DZP+ghosts)	2.002919	66

[a] STO-type DZP(ZORA) basis set was used. [b] Results for BV in the αACDδ•+ protonation state. [c] Nonrelaxed ρ_B. [d] Relaxed ρ_B.

As far as the basis set effect on the obtained complexation induced shifts is concerned, it is worthwhile to notice that the two previously considered choices for the basis sets (monomer or supermolecular expansion) represent two extremes in practical calculations. Most of the QM/MM calculations do not employ the basis sets localized in the environment. From the practical point of view, however, it is more useful to analyze the numerical stability of the shifts obtained from embedding calculations if only the monomer expansion is considered but the atomic basis sets change. The following section addresses this issue for one case: BV in the $\alpha ACD\delta^{\bullet+}$ protonation state in the EHD environment.

We start with noticing that, the complexation induced shifts of iso-g obtained from supermolecular calculations are not affected by the change of the basis set significantly (see Table 3). The basis set superposition error on Δiso-g obtained from the supermolecular strategy is negligible reaching 3 ppm at most (data not shown). Embedding calculations using Coulombic embedding potential appear to be very sensitive to the choice of the basis set. With the monomer expansion, the shifts equal to 35 and 23 ppm for STO-DZ and STO-DZP, respectively. These values represent less than 50% of the reference shifts (72 or 75 ppm). Reducing the size of the basis set on each atom in the supermolecular expansion

form STO-DZP to STO-DZ does not bring solution to the problem of the lack of convergence in the electrostatic-only embedding case.

The shifts obtained from embedding calculations with the full embedding potential are significantly more stable numerically and closer to the reference. With the monomer expansion the corresponding shifts are 72 and 66 ppm, which are also very close to the corresponding supermolecular reference (72 and 75 ppm for STO−DZ and STO−DZP, respectively). Moreover, adding the centers localized in the environment does not affect the obtained shifts significantly. The shifts obtained with four considered sets of basis functions are scattered between 66 and 72 ppm.

The numerical results discussed so far show invariably that the full embedding potential is indispensable for obtaining numerically stable values of complexation induced shifts. However, an important factor in embedding calculations applying the potential given in eq 4 is the choice of the electron density ρ_B. Performing the full "freeze-and-thaw" procedure (SDFT) is not practical in the case of large environments, and a nature of multilevel simulations is that additional approximations are introduced for ρ_B, as in methods based on FDET. In the following part, we focus on the ACD$^{\bullet-}$ case, where nonrelaxed electron density was shown to be a very inappropriate choice for ρ_B, as it leads to a wrong sign of the complexation induced shift of iso-g. Moreover, the difference between the results obtained using the monomolecular and supermolecular expansion in embedding calculations was the largest as well as the effect of relaxation was also the largest in magnitude. We notice that opposite to other complexes considered in the present work, the embedded system was charged, and it was charged negatively. This suggests attribution of the failure of nonrelaxed embedding calculations to the neglect of electronic polarization and to the role of charge transfer between the embedded radical and the environment or even some covalent character of the bonding between the embedded species and its environment. The analysis of the complexation induced dipole moments in this systems supports the attribution of the failure of nonrelaxed ρ_B embedding calculations to the missing electronic polarization (see Table 3). To support this interpretation of the inadequacy of choosing nonrelaxed ρ_B for negatively charged environment of BV, the complexation induced dipole moments collected in Table 4 are analyzed below. The complexation induced shifts are the smallest (2.93 D) if both the embedded species and the environment are not charged, i.e., for ACD$\delta^{\bullet}$. In this case, the embedding calculations reproduce quite reasonably the complexation induced increase of the dipole moment (2.46 vs 2.93 D) but only if relaxation is taken into account. It is worthwhile to notice that despite such under performance in reproducing the complexation induced dipole moments in the absence of relaxation, the shifts of iso-g were very accurately reproduced (153 vs 192 ppm see Table 1) even if nonrelaxed ρ_B is used in embedding calculations. This indicates that the quality of the embedding potential does not affect all properties of the embedded species in the same way. The choice of the simplified method to obtain ρ_B in large scale simulations using eq 4 must, therefore, be subject of dedicated studies depending on the system and the investigated property. Interestingly, the complexation induced dipole moments are only slightly larger for the two cases of cationic embedded species is (3.07 and 3.94 D). Turning back to the ACD$\delta^{\bullet-}$ case, i.e., where the choice of nonrelaxed ρ_B was qualitatively wrong for evaluation of Δiso-g, we notice that the complexation induced dipole moment is, indeed, the largest (7.10 D), and effect of the relaxation of ρ_B on the calculated dipole moment is the largest.

Table 4. Complexation Induced Dipole Moments ($|\Delta\vec{\mu}| = |\vec{\mu}_{BV+env.} - \vec{\mu}_{BV} - \vec{\mu}_{env.}|$) from Embedding and Supermolecular Calculations

method[a]	environment	protonation state of BV	$\lvert\Delta\vec{\mu}\rvert$ (D)
Kohn−Sham	EHD	αACD$\delta^{\bullet+}$	3.07
embedding: eq 4[b]	EHD	αACD$\delta^{\bullet+}$	0.73
embedding: eq 4[c]	EHD	αACD$\delta^{\bullet+}$	2.18
Kohn−Sham	EHDYD[b]	αACD$\delta^{\bullet+}$	3.94
embedding: eq 4[b]	EHDYD	αACD$\delta^{\bullet+}$	1.16
embedding: eq 4[c]	EHDYD	αACD$\delta^{\bullet+}$	1.77
Kohn−Sham	EHD	ACD$\delta^{\bullet}$	2.93
embedding: eq 4[b]	EHD	ACD$\delta^{\bullet}$	0.93
embedding: eq 4[c]	EHD	ACD$\delta^{\bullet}$	2.46
Kohn−Sham	EHD	ACD$^{\bullet-}$	7.10
embedding: eq 4[b]	EHD	ACD$^{\bullet-}$	1.27
embedding: eq 4[c]	EHD	ACD$^{\bullet-}$	5.87

[a] STO-type DZP(ZORA) basis set was used. [b] Nonrelaxed ρ_B. [c] Relaxed ρ_B.

Conclusions

The applicability of the embedding strategy as an alternative to supermolecular calculations was investigated using a small model system comprising BV and a few amino acids of the PCYA protein. The numerical results indicate clearly that the nonelectrostatic components of the embedding potential are indispensable. Without a nonelectrostatic component of the exact embedding potential, the results of embedding calculations are not reliable as the effect of the environment on the investigated property (shift of iso-g) is described erratically (strong dependence of the results on the basis sets) and even qualitatively wrong. The magnitude of the change in iso-g resulting from changing the protonation state of the radical can be significant as estimated in this work and in the work by Stoll et al.[57] (a few hundreds of ppm). Such effects on iso-g are significantly larger in magnitude than the differences between supermolecular and embedding results. Even larger effects on the magnitude of iso-g can be expected to rise from the effect of protein on the conformation of the radical. Both supermolecular or embedding strategies can be, therefore, used to target these larger effects. The present work indicates that if the nonelectrostatic terms are taken into account by approximate density functionals, then the embedding strategy can be considered as a numerically efficient alternative. It is important to underline that neither supermolecular nor embedding calculations are likely to be used for interpretations of very small effects, such as the shift of iso-g of BV resulting from protein mutations which do not exceed 15 ppm.[57] The effect is too small to be reliably predicted by any type of calculations at least for the mutants for which the data is available.

Concerning practical calculations based on the frozen-density embedding theory,[24−28] the analytic form of the nonelectrostatic components of the exact embedding potential is unfortunately not known. Approximants must be used instead. The present work shows that the currently known approximants to these terms perform quite reasonably. The embedding calculations can reproduce the 50−90% of the reference shifts obtained using the supermolecular strategy. The fact that the shifts are not perfectly reproduced indicates that further improvements of the approximants for the kinetic energy-dependent component of the embedding potential are needed. The present work provides also important hints for setting up a large-scale multilevel simulation based on FDET. For the neutral and cationic amino acids interacting with BV, using the nonpolarized electron density to evaluate the orbital-free embedding potential is a reasonable approximation. For negatively charged amino acids, however, the electronic polarization of the environment by the embedded molecule must be taken into account. We underline that the embedding calculations using the orbital-free embedding potential lead to results which are numerically robust and do not vary significantly with the basis sets, even if additional basis sets centered on atoms in the environment are used in construction of embedded orbitals.

Finally, we stress that the practical recommendations and conclusions emerging from the present studies concerning: weak basis set dependence, negligible effect of atomic basis sets localized in the environment, reasonably good approximation of neglecting electronic polarization of neutral and cationic amino acids in the environment, adequacy of the NDSD approximant for the nonadditive kinetic energy were drawn based on the analyses of shifts of the iso-g. Investigation of other properties, the quality of which is directly linked to the accuracy of the used embedding potential, might lead to different recommendations. For instance, the relative errors (deviation from the reference supermolecular results) in the complexation induced dipole moments obtained from embedding calculations do not correlate well with the errors in the iso-g shifts despite the fact that both errors are determined by the quality of the used orbital-free embedding potential. According to our numerical experience, the complexation induced dipole moments are very sensitive to the variations in the embedding potential. This is one of the reasons we use induced dipoles in the methodological studies aimed at development or validation of approximants for the nonadditive kinetic potential.[45−47]

Acknowledgment. This work was supported by the grant 200020-124817 from the Fonds National Suisse de la Recherche Scientifique.

Supporting Information Available: Cartesian coordinates are provided. This material is available free of charge via the Internet at http://pubs.acs.org.

References

(1) Warshel, A.; Levitt, M. *J. Mol. Biol.* **1976**, *103*, 227.

(2) Aqvist, J.; Warshel, A. *Chem. Rev.* **1993**, *93*, 2523.

(3) Senn, H. M.; Thiel, W. *Angew. Chem., Int. Ed.* **2009**, *48*, 1198.

(4) Sauer, J.; Ugliengo, P.; Garrone, E.; Saunders, V. R. *Chem. Rev.* **1994**, *94*, 2095.

(5) Chalmet, S.; Rinaldi, D.; Ruiz-Lopez, M. F. *Int. J. Quantum Chem.* **2001**, *84*, 559.

(6) Sokol, A.; Bromley, S.; French, S.; Catlow, C.; Sherwood, P. *Int. J. Quantum Chem.* **2004**, *99*, 695.

(7) Gao, J. In *Reviews in Computational Chemistry*; Lipkowitz, K. B.; Boyd, D. B., Eds.; VCH: New York, 1995; Vol. 7; pp 119−185.

(8) Ellis, D.; Warschkow, O. *Coord. Chem. Rev.* **2003**, *238*, 31.

(9) Savin, A.; Wesolowski, T. A. *Progress in Theoretical Chemistry and Physics* **2009**, *19*, 327.

(10) Neaton, J. B.; Ashcroft, N. W. *Nature* **1999**, *400*, 141.

(11) Riccardi, D.; Schaefer, P.; Cui, Q. *J. Phys. Chem. B* **2005**, *109*, 17715.

(12) Kastner, J.; Thiel, S.; Senn, H. M.; Sherwood, P.; Thiel, W. *J. Chem. Theory Comput.* **2007**, *3*, 1064.

(13) Murphy, R. B.; Philipp, D. M.; Friesner, R. A. *J. Comput. Chem.* **2000**, *21*, 1442.

(14) Bakowies†, D.; Thiel, W. *J. Phys. Chem.* **1996**, *100*, 10580.

(15) Gao, J.; Amara, P.; Alhambra, C.; Field, M. J. *J. Phys. Chem.* **1998**, *102*, 4714.

(16) Thiel, W. In *Multiscale Simulation Methods in Molecular Sciences*; Grotendorst, J., Attig, N., Blugel, S., Marx, D., Eds.; Institute for Advanced Simulation, Forschungszentrum Julich: Julich, Germany, 2009; NIC Series; Vol. 42; pp 203−214.

(17) Titmuss, S. J.; Cummins, P. L.; Rendell, A. P.; Bliznyuk, A. A.; Gready, J. E. *J. Comput. Chem.* **2002**, *23*, 1314.

(18) Das, D.; Eurenius, K. P.; Billings, E. M.; Sherwood, P.; Chatfield, D. C.; Hodoscek, M.; Brooks, B. R. *J. Chem. Phys.* **2002**, *117*, 10535.

(19) V. Guallar, M.-H. B.; Lippard, S. J.; Friesner, R. A. *Proc. Natl. Acad. Sci. U.S.A.* **2003**, *100*, 6998.

(20) Biswas, P. K.; Gogonea, V. *J. Chem. Phys.* **2005**, *123*, 164114.

(21) Laio, A.; VandeVondele, J.; Rothlisberger, U. *J. Chem. Phys.* **2002**, *116*, 6941.

(22) Tu, Y.; Laaksonen, A. *J. Chem. Phys.* **1999**, *111*, 7520.

(23) Tunon, I.; Martins-Costa, M. T.; Millot, C.; Ruiz-Lopez, M. F. *Chem. Phys. Lett.* **1995**, *241*, 450.

(24) Wesolowski, T. A.; Warshel, A. *J. Phys. Chem.* **1993**, *97*, 8050.

(25) Wesolowski, T. A. *J. Am. Chem. Soc.* **2004**, *126*, 11444.

(26) Wesolowski, T. A. In *Computational Chemistry: Reviews of Current Trends*; Leszczynski, J., Ed.; World Scientific: Singapore, 2006; Vol. X; pp 1−82.

(27) Wesolowski, T. A. *Phys. Rev. A* **2008**, *77*, 012504.

(28) Pernal, K.; Wesolowski, T. A. *Int. J. Quantum Chem.* **2009**, *109*, 2520.

(29) Stefanovich, E. V.; Truong, T. N. *J. Chem. Phys.* **1996**, *104*, 2946.

(30) Govind, N.; Wang, Y. A.; Carter, E. A. *J. Chem. Phys.* **1999**, *110*, 7677.

(31) Neugebauer, J.; Baerends, E. J. *Phys. Rev. A: At., Mol., Opt. Phys.* **2006**, *110*, 8786.

(32) Hodak, M.; Lu, W.; Bernholc, J. *J. Chem. Phys.* **2008**, *128*, 014101.

(33) Gomes, A. S. P.; Jacob, C. R.; Visscher, L. *Phys. Chem. Chem. Phys.* **2008**, *10*, 5353.

(34) Kohn, W.; Sham, L. J. *Phys. Rev.* **1965**, *140*, A1133.

(35) Hohenberg, P.; Kohn, W. *Phys. Rev.* **1964**, *136*, B864.

(36) Cortona, P. *Phys. Rev. B: Condens. Matter Mater. Phys.* **1991**, *44*, 8454.

(37) Senatore, G.; Subbaswamy, K. *Phys. Rev. B: Condens. Matter Mater. Phys.* **1986**, *34*, 5754.

(38) Elliott, P.; Cohen, M. H.; Wasserman, A.; Burke, K. *J. Chem. Theory and Comput.* **2009**, *5*, 827.

(39) Wesolowski, T. A.; Chermette, H.; Weber, J. *J. Chem. Phys.* **1996**, *105*, 9182.

(40) Wesolowski, T. A.; Tran, F. *J. Chem. Phys.* **2003**, *118*, 2072.

(41) Kevorkyants, R.; Dulak, M.; Wesolowski, T. A. *J. Chem. Phys.* **2006**, *124*, 024104.

(42) Dulak, M.; Kaminski, J. W.; Wesolowski, T. A. *J. Chem. Theory Comput.* **2007**, *3*, 735.

(43) Iannuzzi, M.; Kirchner, B.; Hutter, J. *Chem. Phys. Lett.* **2006**, *421*, 16.

(44) Dulak, M.; Kaminski, J. W.; Wesolowski, T. A. *Int. J. Quant. Chem.* **2009**, *109*, 1886.

(45) Wesolowski, T. A.; Weber, J. *Int. J. Quantum Chem.* **1997**, *61*, 303.

(46) Lastra, J. M. G.; Kaminski, J. W.; Wesolowski, T. A. *J. Chem. Phys.* **2008**, *129*, 074107.

(47) Bernard, Y. A.; Dulak, M.; Kaminski, J. W.; Wesolowski, T. A. *J. Phys. A* **2008**, *41*, 0553902.

(48) Fradelos, G.; Kaminski, J. W.; Wesolowski, T. A.; Leutwyler, S. *J. Phys. Chem. A* **2009**, *19*, 9766.

(49) Wesolowski, T. A. *Chem. Phys. Lett.* **1999**, *311*, 87.

(50) Neugebauer, J.; Louwerse, M. J.; Belanzoni, P.; Wesolowski, T. A.; Baerends, E. J. *J. Chem. Phys.* **2005**, *123*, 114101.

(51) Zbiri, M.; Atanasov, M.; Daul, C.; Garcia-Lastra, J. M.; Wesolowski, T. A. *Chem. Phys. Lett.* **2004**, *397*, 441.

(52) Jacob, C. R.; Visscher, L. *J. Chem. Phys.* **2006**, *125*, 194104.

(53) Jacob, C. J.; Neugebauer, J.; Jensen, L.; Visscher, L. *Phys. Chem. Chem. Phys.* **2006**, *8*, 2349.

(54) Kaminski, J. W.; Gusarov, S.; Kovalenko, A.; Wesolowski, T. A. *J. Phys. Chem. A* **2010**, *114*, 6082.

(55) Wesolowski, T. A.; Weber, J. *Chem. Phys. Lett.* **1996**, *248*, 71.

(56) Dulak, M.; Wesolowski, T. A. *J. Chem. Phys.* **2006**, *124*, 164101.

(57) Stoll, S.; Gunn, A.; Brynda, M.; Sughrue, W.; Kohler, A. C.; Ozarowski, A.; Fisher, A. J.; Lagarias, J. C.; Britt, R. D. *J. Am. Chem. Soc.* **2009**, *131*, 1986.

(58) Hagiwara, Y.; Sugishima, M.; Takahashi, Y.; Fukuyama, K. *Proc. Natl. Acad. Sci. U.S.A.* **2006**, *103*, 27.

(59) Tu, S. L.; Gunn, A.; Toney, M. D.; Britt, R. D.; Lagarias, J. C. *J. Am. Chem. Soc.* **2004**, *126*, 8682.

(60) *Accelrys DS Visualizer*, v2.0.1.7347; Accelrys Software Inc.: San Diego, CA, 2007.

(61) Boys, S. F.; Bernardi, F. *Mol. Phys.* **2002**, *100*, 65.

(62) Dulak, M.; Wesolowski, T. A. *Int. J. Quantum Chem.* **2005**, *101*, 543.

(63) Jacob, C. R.; Wesolowski, T. A.; Visscher, L. *J. Chem. Phys.* **2005**, *123*, 174104.

(64) Wesolowski, T. A. *J. Chem. Phys.* **1997**, *106*, 8516.

(65) Knowles, P., Marsh, D., Rattle, H. *Magnetic Resonance of Biomolecules*; Wiley:London, U.K., 1976.

(66) van Lenthe, E.; Baerends, E. J.; Snijders, J. G. *J. Chem. Phys.* **1993**, *99*, 4597.

(67) van Lenthe, E.; Baerends, E. J.; Snijders, J. G. *J. Chem. Phys.* **1994**, *101*, 9783.

(68) van Lenthe, E.; van Leeuwen, R.; Baerends, E.; Snijders, J. *Intl. J. Quantum Chem.* **1996**, *57*, 281.

(69) van Lenthe, E.; Snijders, J.; Baerends, E. *J. Chem. Phys.* **1994**, *105*, 6505.

(70) van Lenthe, E.; van der Avoird, A.; Wormer, P. *J. Chem. Phys.* **1997**, *107*, 2488.

(71) van Lenthe, E.; van der Avoird, A.; Wormer, P. *J. Chem. Phys.* **1998**, *108*, 4783.

(72) Becke, A. D. *Phys. Rev. A: At., Mol., Opt. Phys.* **1988**, *38*, 3098.

(73) Perdew, J. P. *Phys. Rev. B: Condens. Matter Mater. Phys.* **1986**, *33*, 8822.

(74) *ADF 2009 suite of programs*; Theoretical Chemistry Department, Vrije Universiteit: Amsterdam, The Netherlands; http://www.scm.com. Accessed October 21, 2010.

CT100415H